

## Quantum dynamical simulations of local field enhancement in metal nanoparticles

This article has been downloaded from IOPscience. Please scroll down to see the full text article.

2013 J. Phys.: Condens. Matter 25 125304

(<http://iopscience.iop.org/0953-8984/25/12/125304>)

View [the table of contents for this issue](#), or go to the [journal homepage](#) for more

Download details:

IP Address: 200.16.16.13

The article was downloaded on 08/05/2013 at 21:58

Please note that [terms and conditions apply](#).

# Quantum dynamical simulations of local field enhancement in metal nanoparticles

Christian F A Negre<sup>1</sup>, Eduardo M Perassi<sup>2</sup>, Eduardo A Coronado<sup>2</sup> and Cristián G Sánchez<sup>1</sup>

<sup>1</sup> Departamento de Matemática y Física, Facultad de Ciencias Químicas, INFIQC, Universidad Nacional de Córdoba, Ciudad Universitaria, X5000HUA, Córdoba, Argentina

<sup>2</sup> Departamento de Fisicoquímica, Facultad de Ciencias Químicas, INFIQC, Universidad Nacional de Córdoba, Ciudad Universitaria, 5000, Córdoba, Argentina

E-mail: [cgsanchez@fcq.unc.edu.ar](mailto:cgsanchez@fcq.unc.edu.ar)

Received 23 November 2012, in final form 29 January 2013

Published 28 February 2013

Online at [stacks.iop.org/JPhysCM/25/125304](http://stacks.iop.org/JPhysCM/25/125304)

## Abstract

Field enhancements ( $\Gamma$ ) around small Ag nanoparticles (NPs) are calculated using a quantum dynamical simulation formalism and the results are compared with electrodynamic simulations using the discrete dipole approximation (DDA) in order to address the important issue of the intrinsic atomistic structure of NPs. Quite remarkably, in both quantum and classical approaches the highest values of  $\Gamma$  are located in the same regions around single NPs. However, by introducing a complete atomistic description of the metallic NPs in optical simulations, a different pattern of the  $\Gamma$  distribution is obtained. Knowing the correct pattern of the  $\Gamma$  distribution around NPs is crucial for understanding the spectroscopic features of molecules inside hot spots. The enhancement produced by surface plasmon coupling is studied by using both approaches in NP dimers for different inter-particle distances. The results show that the trend of the variation of  $\Gamma$  versus inter-particle distance is different for classical and quantum simulations. This difference is explained in terms of a charge transfer mechanism that cannot be obtained with classical electrostatics. Finally, time dependent distribution of the enhancement factor is simulated by introducing a time dependent field perturbation into the Hamiltonian, allowing an assessment of the localized surface plasmon resonance quantum dynamics.

(Some figures may appear in colour only in the online journal)

## 1. Introduction

Electromagnetic field enhancements around metal nanoparticles (NPs) produced by localized surface plasmon resonance (LSPR) is currently the subject of a great number of research studies due to the huge impact that this effect has in many different applications. The most direct application is in the field of enhanced spectroscopic techniques such as SERS (surface enhanced Raman spectroscopy) [1–7], SM-SERS (single molecule surface enhanced Raman spectroscopy) [8–16], TERS (tip enhanced Raman spectroscopy) [17–26] and SEF (surface enhancement fluorescence) [27–29]. Likewise, they are also of importance in other experimental techniques such as nanolithography [30–33], SNOM (scanning near field optical microscopy) [34, 35], biosensors [36–39] and

chemical sensor design [40], just to mention the most relevant ones.

A rigorous theoretical determination of the  $\Gamma$  distribution around metal NPs remains an important issue for understanding and therefore optimizing the performance and design of LSPR devices. Electrodynamic methods have been shown to be powerful tools for describing the optical properties of metallic NPs and nanostructures [41, 42]. However, the main shortcoming of this approach is that matter is considered as a continuum and therefore the intrinsic atomistic structure of matter is lost. On the other hand, studies have been done that indirectly include quantum effects in classical electrodynamic simulation by using a non-local effect in the dielectric constant [43] and taking into account electron confinement effects (surface scattering) [44].

Recent efforts have been devoted to including quantum effects in the calculation of the optical properties of NPs by extending the TDDFT (time dependent density functional theory) quantum approach to nanostructures where a jellium model is used. Through these calculations new phenomena in the optical behavior showing tunneling effects between two close NPs were elucidated for small nanostructures [45, 46]. However in these calculations the atomistic nature of matter is again not considered. Although TDDFT should be the most suitable approach [47, 48] for calculating near field optical properties, it might become computationally unaffordable for particles sizes of the order of hundreds of atoms.

In this work, we calculate  $\Gamma$  distributions around small Ag NPs including both quantum effects and metal structure at an atomistic level and the results are compared with electrodynamics calculations using the discrete dipole approximation (DDA) with quantum corrections. This constitute a direct comparison of a quantum atomistic versus a classical continuum method.

## 2. Theoretical methods

The study was performed on NPs corresponding to stable thermodynamic structures [49]. The model used for the quantum calculation approach is based on a time dependent self-consistent density functional tight-binding simulation (TDDFTB). The self-consistent density functional tight-binding method (SCC-DFTB) is an efficient scheme for describing the electronic structure of large systems [50]. It is based on the second order expansion of the Kohn–Sham energy functional around a reference density of neutral atomic species. The DFTB+ code [51] is a computational implementation of the DFTB method. We have used this code as obtained from the authors to calculate Hamiltonian and overlap matrix elements as well as the initial single electron density matrix. Several different incarnations of time dependent SCC-DFTB have been described in the literature, both within linear response [52, 53] and implementing the full non-linear dynamics [54]. Our implementation differs from that of [54] in that it propagates the one electron density matrix instead of single particle orbitals.

The SCC-DFTB Hamiltonian is an intermediate step between a simple tight-binding Hamiltonian and a fully *ab initio* density functional theory (DFT) representation of the electronic structure. The Hamiltonian matrix elements are obtained as follows [50]:

$$H_{\mu\nu} = \langle \phi_\mu | \hat{H}^0 | \phi_\nu \rangle + \frac{1}{2} S_{\mu\nu} \sum_k^N (\gamma_{ik} + \gamma_{jk}) \Delta q_k \quad (1)$$

where orbitals  $\mu$  and  $\nu$  belong to atoms  $i$  and  $j$ , respectively. Here,  $\Delta q_k = q_k - q_k^0$  is the difference between the charge of the isolated atom  $q_k^0$  and the charge  $q_k$  obtained by Mulliken population analysis when atom  $k$  is conforming the molecule. The function of inter-atomic separation  $\gamma_{ij} = \gamma_{ij}(U_i, U_j, |\vec{R}_i - \vec{R}_j|)$ , interpolates smoothly between on-site interactions with a strength  $U_i = \gamma_{ii}$  and the bare Coulomb interaction at large separation. The latter parameter is related

to the chemical hardness of the atomic species. Here,  $S_{\mu\nu} = \langle \phi_\mu | \phi_\nu \rangle$  are the overlap matrix elements and  $H_{\mu\nu}^0$  are the matrix elements of the non-SCC-TB Hamiltonian within the Slater–Koster parametrization.  $H_{\mu\nu}^0$  and  $S_{\mu\nu}$  are calculated from first principles for a minimal Slater orbital basis and tabulated for all pairs of species. For the calculations shown here we have used the ‘hyb-0-2’ parameter set [50] for silver. The DFTB method has been extensively validated for the prediction of molecular structures and reaction energies [55]. The prediction of optical properties and simulations of any real time quantum dynamical properties is outside the application for which the method was initially proposed and it has only very recently been applied to this area [56–59]. In this respect the method inherits both the successes (and failures) of time dependent density functional theory, but at a much lower computational cost [60].

Mulliken charges  $q_i$  are obtained by summing over every orbital contribution as follows:

$$q_i = \frac{1}{2} \sum_K^{\text{occ}} n_K \sum_{\mu \in i} \sum_v^N (c_{\mu K}^* c_{v K} S_{\mu\nu} + c_{v K}^* c_{\mu K} S_{v\mu}) \quad (2)$$

where  $n_K$  are the molecular orbital fillings and  $c_{\mu K}$  are the expansion coefficients of  $\psi_{\text{GS}}$  obtained by solving the eigenvalue problem in the atomic orbital basis. In matrix notation we have

$$q_i = \frac{1}{2} \sum_{\mu \in i} (\rho S + S \rho)_{\mu\mu} \quad (3)$$

where  $\rho_{\mu\nu} = \sum_K^{\text{occ}} c_{\mu K}^* n_K c_{\nu K}$  is the one electron density matrix.

For the quantum simulations we first perform a determination of the self-consistent DFTB Hamiltonian and the one electron density matrix for the system ground state (GS). This task is carried out by using the DFTB+ code as provided by the authors. At  $t > t_0$  we apply an external field (of  $0.01 \text{ V \AA}^{-1}$ ) in a short time interval (0.05 fs) to the initial GS density matrix previously obtained [61]. The Hamiltonian is in consequence modified accordingly:  $\hat{H} = \hat{H}^0 + \mathbf{E}_0 \theta(t - t_0) \hat{\rho}$ . When the initial applied electric fields are small, the system responds within the linear response regime. After the application of the field, the density matrix evolves in time and its evolution can be calculated by time integration of the Liouville–Von Neumann equation of motion in the non-orthogonal basis:

$$\frac{\partial \hat{\rho}}{\partial t} = \frac{1}{i\hbar} \left( S^{-1} \hat{H}[\hat{\rho}] \hat{\rho} - \hat{\rho} \hat{H}[\hat{\rho}] S^{-1} \right). \quad (4)$$

This model may be viewed as an intermediate step before time dependent density functional theory (TDDFT) in the adiabatic local density approximation (ALDA) [62] and it was recently applied for calculating the optical properties of biological pigments [56, 57]. Note that  $\hat{H}$  depends on  $\hat{\rho}$  through the on-site charges introducing non-linear effects in the dynamics, renormalizing the excitations of the non-self-consistent DFTB Hamiltonian [54].

The electric field induced by plasmonic oscillations can be calculated at any space point using the following

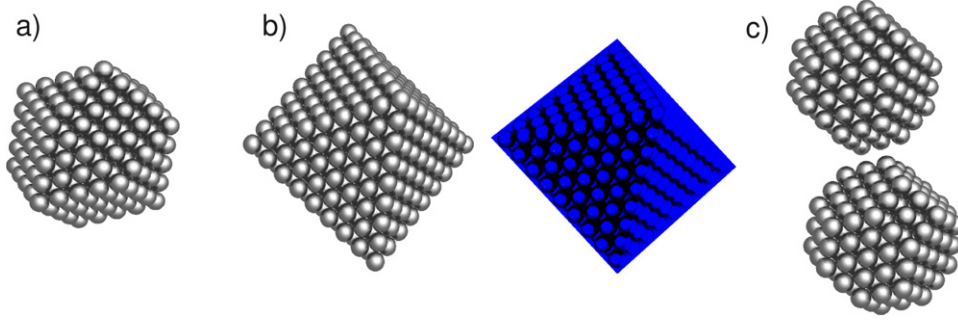


**Figure 1.** Analyzed clusters. (a) Cubooctahedron with 309 silver atoms. (b) Octahedron with 489 silver atoms (left). Classical volume (blue) overlaid with the quantum volume (spheres) for the case of the octahedron (right). (c) Dimer of two truncated octahedra with 201 silver atoms each.

expression:

$$\mathbf{E}(\mathbf{r}) = \sum_i \frac{\Delta q_i}{4\pi\epsilon^0} \frac{(\mathbf{r}_i - \mathbf{r})}{\|\mathbf{r}_i - \mathbf{r}\|^3}. \quad (5)$$

and  $\Gamma$  is calculated as follows:

$$\Gamma = \frac{|\mathbf{E}|^2(\omega)}{|\mathbf{E}_{\text{appl}}|^2(\omega)} \quad (6)$$

where the applied field has the form  $\mathbf{E}_{\text{appl}}(t) = (\theta(t - t_0))\mathbf{E}_0$  in the time domain. This value is directly related to the Raman signal amplification [63]. We have checked that enhancement factors are independent of the initial applied field intensity  $\mathbf{E}_0$  satisfying the conditions for a linear response regime.

Classical electrodynamics simulations were performed by using the DDA method [64] which allows the simulations of NPs with non-analytical geometry [65] and has been demonstrated to give very good agreement with experiments. Briefly, in this method the object of interest is an array of  $N$  cubic polarizable volume elements and the optical response of this array is determined by solving in a self-consistent way the induced dipole moments in each element. The  $\Gamma$  distributions around the NPs were calculated by using dipole probes [66] and the convergence analysis of the calculations was checked using a recently developed variation of the trapped volume (VTV) approach [66]. In this simulation the silver dielectric constant as tabulated by Palik [67] was used. For describing perfect crystalline Ag NPs the dielectric constant of Johnson and Christy is better [68] than that given in Palik; however, for the purpose of this work the dielectric constant of Palik is more appropriate.

The effect of electron surface scattering was introduced into the dielectric constant [44] using the following correction to the damping parameter  $\gamma$  in the Drude free electron model

$$\gamma(L_{\text{eff}}) = \gamma_0 + A \frac{v_F}{L_{\text{eff}}} \quad (7)$$

where  $A$  is a dimensionless parameter that is determined by details of the scattering process and is here assumed to be equal to 0.25 [69],  $v_F$  is the Fermi velocity and  $L_{\text{eff}}$  is the effective mean free path obtained from

$$L_{\text{eff}} = \frac{4V}{S} \quad (8)$$

$V$  being the volume and  $S$  the surface of the NP.

### 3. Absorption spectrum simulation

For very small applied electric fields (linear response regime), the time dependent dipole moment arising from the quantum dynamics simulation can be expressed as

$$\mu(t) = \int_{-\infty}^{\infty} \alpha(t - \tau)\mathbf{E}(\tau)\Theta(t - \tau)d\tau \quad (9)$$

where  $\mathbf{E}(\tau)$  is the applied electric field and  $\alpha(t - \tau)$  is the time dependent polarizability. Written in the frequency domain, the last expression reads

$$\mu(\omega) = \alpha(\omega)\mathbf{E}(\omega). \quad (10)$$

The absorption spectrum is then proportional to  $\alpha(\omega)$  which is obtained by Fourier transforming the time dependent dipole moment followed by deconvolution of the applied electric field. In this particular case we have employed a pulse-shaped ( $\mathbf{E}_{\text{appl}}(t) = \delta(t - t_0)\mathbf{E}_0$  with  $\mathbf{E}_0 = 0.01 \text{ V \AA}^{-1}$ ) electric field perturbation. The average of the polarizability along the three Cartesian axes was taken as the absorption spectrum of the system. The absorption spectra calculated in this manner were checked to be independent of the applied field (linear response regime), which allows us to extract the  $\alpha(\omega)$  from equation (10). Calculated spectra for the clusters used in this work are shown in figure 2.

### 4. Quantum and classical comparison

Figure 1 shows representations of the atomic structure of Ag NPs studied here which correspond to a cubooctahedron, octahedron and a dimer of truncated octahedra. Figure 2 shows the absorption spectra calculated as explained before for the three systems of figure 1. All the spectra show a single peak with very low absorption at longer wavelength but some non-zero absorption at shorter wavelength, in good agreement with experiments [70]. However, the peak position seems slightly red-shifted compared to previous TDDFT results [71]. These differences could be due to limitations of the TDDFTB technique arising from either an overestimation of the polarizability of core electrons (this can have a strong influence in the position of the absorption peak as demonstrated in [72]) or the typical DFT-inherited underestimation of the energy gap of the frontier orbitals [73].

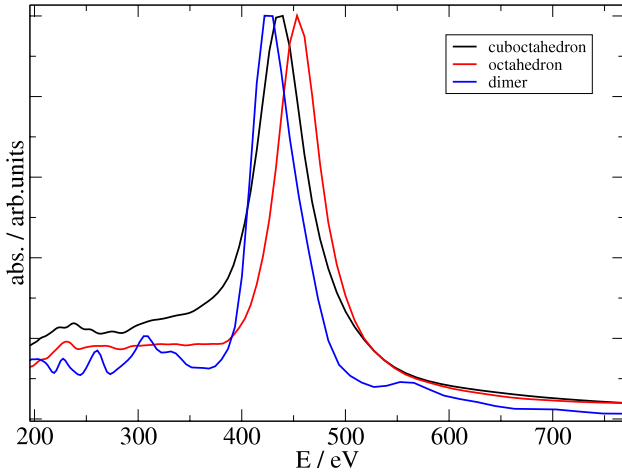


**Figure 2.** Absorption spectra for the systems used here: cuboctahedron with 309 silver atoms (black), octahedron with 489 silver atoms (red) and a dimer of two truncated octahedra with 201 silver atoms each (blue).

In order to compare classical electrodynamical and quantum calculations it is necessary to define a suitable external surface around the NP. In this work we have considered the external surface to be at a distance of 1.4 Å apart from the edges defined by the atomic positions. The value of 1.4 Å stands for Ag atomic radius. Figure 1(b) shows the classical surface (blue filled area) wrapping the atomistic structure for the octahedral NP.

The first case analyzed here is the 309 Ag atom cuboctahedral NP. Figure 3 compares the result of quantum and classical simulations of the  $\Gamma$  distributions taken on a cross section of a cutting plane passing through the center of mass of the NP. For the classical simulation (figure 3(b)) a mesh parameter of  $d \approx 0.0175$  nm is used in order to reach convergence of the DDA calculation analyzed by the VTV approach. Both simulations were performed at the wavelengths that produce the highest values of  $\Gamma$  around the NP which are  $\lambda = 436$  nm and  $\lambda = 395$  nm for quantum and

classical simulations, respectively. The incident polarization and wave propagation vectors are also indicated. In order to make comparison easier, the distributions values of  $\Gamma > 20$  were assigned to the upper bound (red color) of the  $\Gamma$ -color scale. Quite remarkably, both simulations result in general in a very similar local field enhancement distribution: In both distributions the highest values of  $\Gamma$  are localized on the vertices and the area occupied for  $\Gamma > 20$  (red color) is quite similar for both approaches. However, a closer inspection of the distributions indicates that there are some features intrinsic to the atomistic structure [70] that the classical approach is not able to reproduce (figure 3(a)). For example, the hot spots in the quantum results are located mostly in the direction of the polarization, whereas the classical enhancement is evenly distributed around the vertices. The differences in the pattern shown between the two approaches may have a crucial importance when analyzing, for example, the spectroscopic enhancement of a molecule inside the hot spot.

The second case studied here is a 489 Ag atom octahedral NP. The  $\Gamma$  distributions on the cross section of the cutting plane obtained for both quantum and classical calculations are shown in figure 4. Here, the distribution was truncated to  $\Gamma = 50$  in order to properly compare both approaches and, similar to the previous example analyzed, simulations were performed at the wavelengths that give rise to the highest values of  $\Gamma$  around the NP ( $\lambda = 454$  nm and  $\lambda = 424$  nm for quantum and classical simulation, respectively). A mesh parameter of  $d \approx 0.035$  nm was small enough to reach convergence as demonstrated by the VTV analysis approach. The incident polarization and propagation vectors are also indicated in figure 4.

The highest values of  $\Gamma$  are localized at the tips of the octahedron for both quantum and classical results. The fields are also equally aligned along the incident polarization direction. However, the pattern of highest  $\Gamma$  values for the quantum approach is extended over a larger area than in the classical one, and the shape of this pattern seems to be spherical as for the quantum approach, while having an arrow like shape for the classical approach. The quantum result

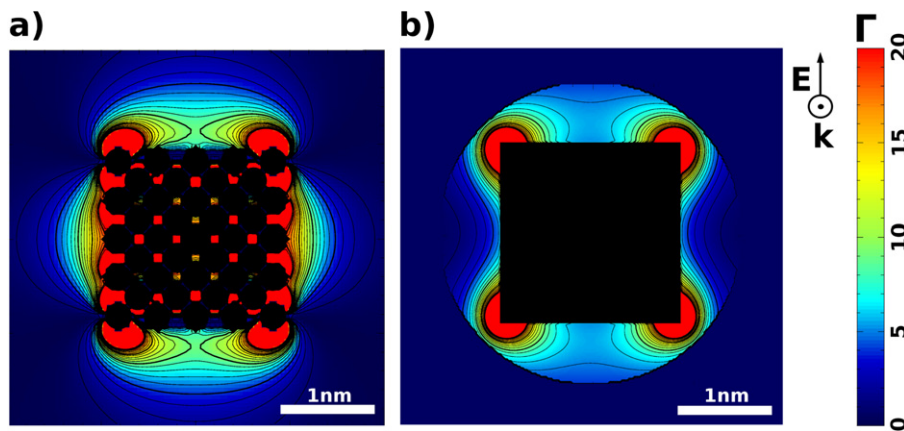


**Figure 3.** Local field enhancement  $\Gamma$  for a transverse cut. Comparison between quantum and classical simulations for a 309 Ag atom cuboctahedron. (a) Quantum TDDFTB simulations. (b) Classical DDA simulation. The electromagnetic field inside the NP has been set to zero in order to identify the NP boundaries.

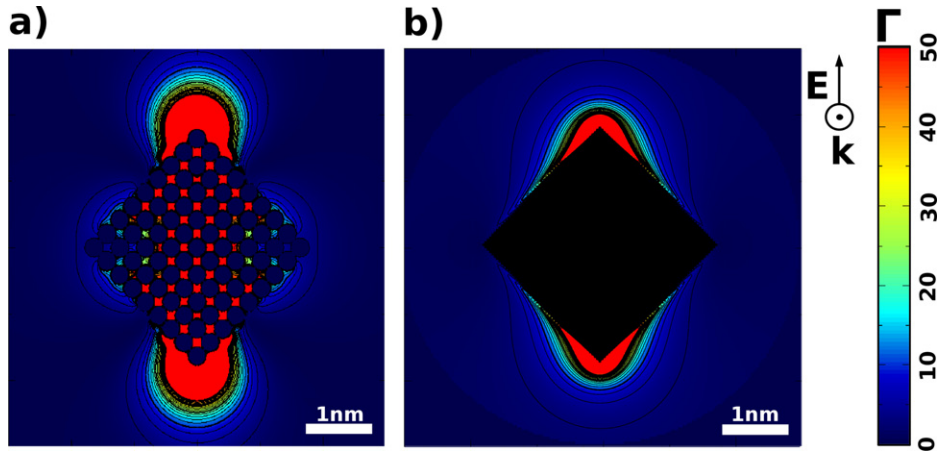


**Figure 4.** Local field enhancement  $\Gamma$  for a transverse cut. Comparison between quantum and classical simulations of a 489 Ag atom octahedron. (a) Quantum TDDFTB simulations. (b) Classical DDA simulation. The electromagnetic field inside the NP has been set to zero in order to identify the NP boundaries.

indicates that, even with small clusters, it should be possible to have extended hot spots and large values of  $\Gamma$ , provided that the curvature on the NP surface is sharp enough. This feature is another issue that could be interesting to test by means of experiments for this particular shape.

In order to address the influence of including the atomistic structure and quantum effects in LSPR coupling, we will now compare the enhancement between NP dimers for both approaches. For this purpose a dimer of two truncated octahedra with 201 Ag atoms is considered. The  $\Gamma$  distribution in between the NPs is calculated for different values of inter-particle distance in order to vary the degree of the LSPR coupling strength. The  $\Gamma$  distributions for the quantum and classical approach on a plane that passes through the major axis of the dimer is depicted in figure 5. Values for inter-particle distances are  $1.5s$ ,  $2s$ ,  $2.5s$ ,  $3s$  and  $4s$ , where  $s$

is the first neighbor distance which is  $2.89 \text{ \AA}$  for the case of Ag. The incident polarization direction (taken to be aligned to the major axis of the dimer) and the wave propagation vector are both indicated on the figure. After a VTV convergence analysis, a mesh parameter of  $d \approx 0.035 \text{ nm}$  was used for the DDA calculations. The wavelengths used in this case were 425 and 422 nm for the quantum and classical approach, respectively, in order to produce the highest values of  $\Gamma$  between the NPs. Again in order to easily compare both distribution values, the color at  $\Gamma = 600$  was assigned for  $\Gamma > 600$ .

On the one hand, figure 5 shows that the highest values of  $\Gamma$  are located in the gap between the NPs for both quantum (figure 5(a)) and classical (figure 5(b)) calculations. Note that these high  $\Gamma$  values seem to have the same distribution for both approaches. On the other hand an

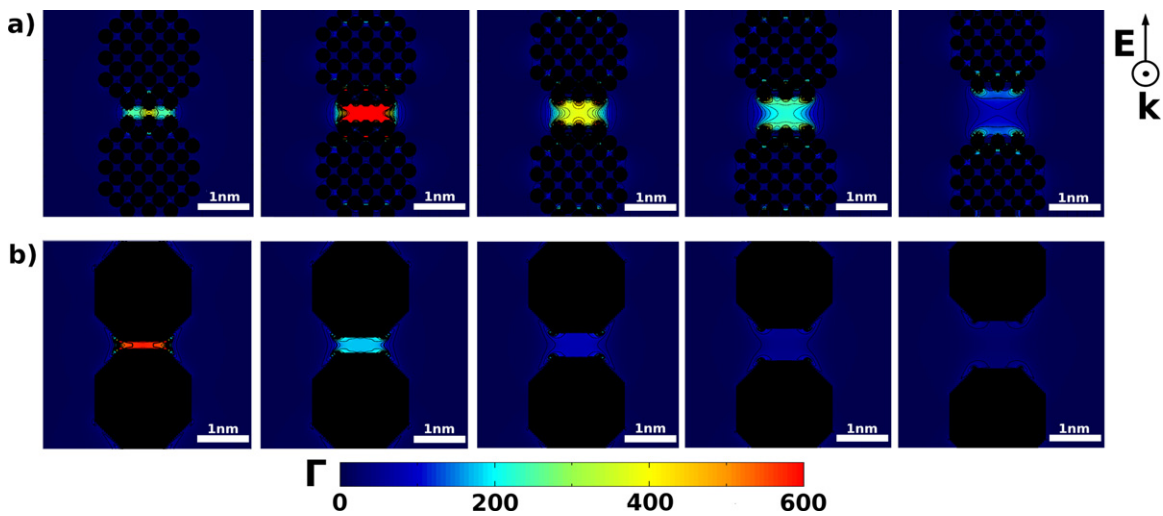


**Figure 5.** Local field enhancement  $\Gamma$  for a transverse cut in truncated octahedral NP dimers of 201 Ag atoms, separated by  $1.5s$ ,  $2.0s$ ,  $2.5s$ ,  $3.0s$  and  $4.0s$ , from left to right, where  $s$  is the first neighbor distance, which for the case of face centered cubic Ag is  $2.89 \text{ \AA}$ . This was done for (a) quantum and (b) classical simulation. The electromagnetic field inside the NP has been set to zero in order to identify the NP boundaries.

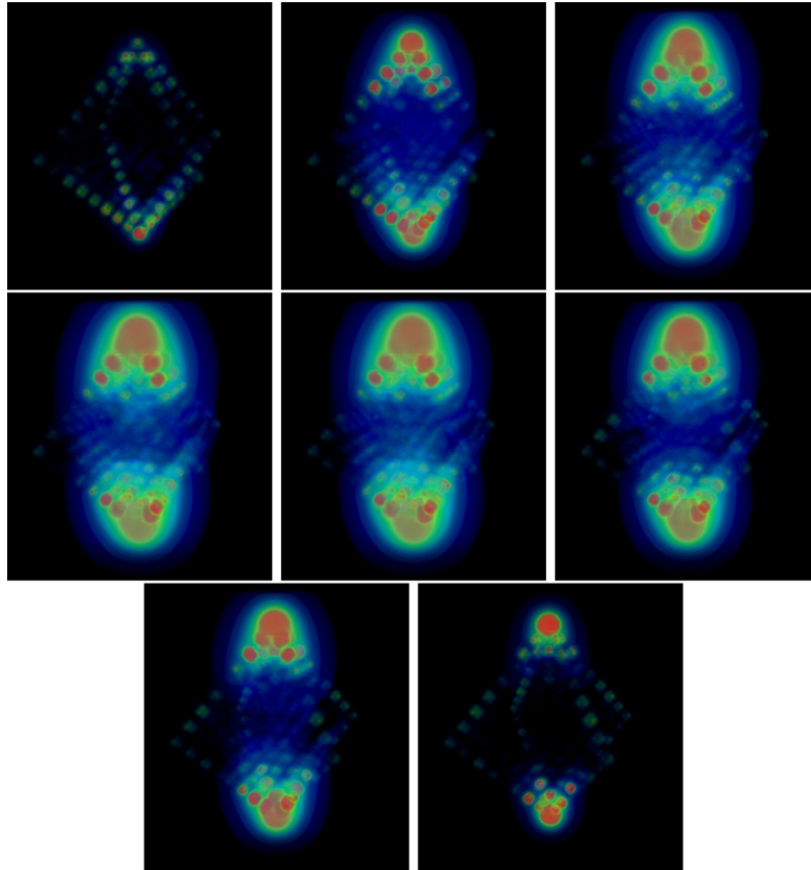


**Figure 6.**  $\Gamma$  value distribution (arbitrary units) calculated during time evolution for a plasmon half-oscillation period when an oscillating field perturbation strikes on a 489 Ag atom octahedron. The wavelength of the oscillating field is 454 nm. The first frame is taken after an illumination time of 93 fs and the snapshots are taken every 0.087 fs. From left to right, the first four frames show the first quarter plasmon oscillation period (enhancing period) whereas the other frames show the second quarter plasmon oscillation period (reduction period).

important feature depicted in figure 5(a) is the different trend of  $\Gamma$  values with inter-particle separation when comparing the classical and quantum calculations in figure 5(b). While in the classical calculation  $\Gamma$  always increases while the inter-particle separation decreases, in the quantum calculation  $\Gamma$  increases as the inter-particle separation decreases up to a critical distance, from which it starts to decrease.

This critical distance corresponds to approximately twice the first nearest neighbor separation  $s$  (see figure 5) which is in agreement with previous quantum jellium results [45]. The existence of an optimal inter-particle separation for which enhancement is a maximum can be explained in terms of electron current flowing during LSPR that can only be taken into account using the quantum approach. The almost zero enhancement when the inter-particle distance is  $s$  can be rationalized by realizing that at this distance the particles are in chemical contact. This result is in good agreement with experimental measurements [74] and simulations employing TDDFT [45].

At large inter-particle distances, where the bonding effect is no longer significant, both approaches show the same behavior and the enhancement values decrease as the inter-particle distance is increased.

Spatiotemporal control over localized plasmons has been demonstrated for femtosecond lasers [75]. In order

to achieve deterministic control for localized plasmons or surface plasmon-polaritons (SPPs) at nanostructures, temporal characterization of femtosecond plasmons is highly required [76]. In this quantum formalism the near-field response of a nanostructure to an arbitrarily shaped laser pulse is easily obtained by only modifying the function  $\mathbf{E}(t)$  in the initial Hamiltonian  $\hat{H}^0$ . For example, for a temporal characterization of an oscillating field as a perturbation, this function should be

$$\mathbf{E}(t) = E_0 \sin\left(\frac{E}{\hbar}t\right). \quad (11)$$

The energy  $E = 2.73$  eV (454 nm) is chosen in such a way as to be in tune with the peak position of the absorption spectrum. This perturbation has been applied to the octahedral NP (figure 1(b)) and it is found that the field increases with time during the application of the perturbation, as can be expected.

Figure 6 shows the  $\Gamma$  distribution around the octahedron at different times after the perturbation is applied.

From left to right, the frames of figure 6 correspond to the first half of the plasmon oscillation. During the first quarter of plasmon oscillation there is an enhancement of the field  $E_0$  due to polarization, as the first four snapshots (from left to right) of figure 6 show. In the second quarter, the further

depolarization produces a decrease of the field. This effect is appreciated in the last four frames (from left to right) of figure 6. These cycles of polarization and depolarization will be repeated during plasmon excitation. By being able to recover the plasmon effect, we aim to show that the present tool can also be used to study transient field enhancement effects.

## 5. Conclusions

In this work we have performed calculations of the enhancement around NPs including atomistic structures by using a time dependent self-consistent density functional tight-binding method (SCC-DFTB) and compared these quantum calculations with electrodynamic simulations including electron quantum confinement effects. The results shown for both approaches demonstrate that there is a fairly good agreement between the magnitude and distribution of the enhancements around the NPs.

Performing quantum calculation with an atomistic description of the NPs gives rise to subtle changes on the  $\Gamma$  distributions around NPs that cannot be reproduced by classical calculations. These differences are of great importance for the understanding of the spectroscopic behavior of a molecule located within a hot spot and the present calculations open up the way for further experimental studies able to account for the differences reported.

Another important effect is obtained for NP dimers, where the  $\Gamma$  distributions between the NPs calculated by the quantum approach show a maximum enhancement for a specific inter-particle separation which is not predicted by the classical approach. Finally, a time dependent perturbation has been introduced in the Hamiltonian in order to obtain the time dependent distributions of enhancement factors around octahedral NPs. This time dependent simulations demonstrates the capability of the present tool to study the temporal near-field response of a nanostructure to an arbitrarily shaped electric field.

## Acknowledgments

We acknowledge support by Consejo Nacional de Investigaciones Científicas y Técnicas (CONICET) through grant PIP 112-200801-000983 and ANPCYT through the grant program BID 1728/OC-AR PICT no. 629 and PME-2006-01581. CFAN and EAP are grateful for studentships from CONICET. Both the first and second authors contributed equally to this work.

## References

- [1] Stiles P L, Dieringer J A, Shah N C and Van Duyne R P 2008 Surface-enhanced Raman spectroscopy *Annu. Rev. Anal. Chem.* **1** 601–26
- [2] Lee S J, Guan Z, Xu H and Moskovits M 2007 Surface-enhanced Raman spectroscopy and nanogeometry: the plasmonic origin of SERS *J. Phys. Chem. C* **111** 17985–8
- [3] Le F, Brandl D W, Urzhumov Y A, Wang H, Kundu J, Aizpurua J, Halas N J and Nordlander P 2008 Metallic nanoparticle arrays: a common substrate for both surface-enhanced Raman scattering and surface-enhanced infrared absorption *ACS Nano* **2** 707–18
- [4] Haynes C L and Van Duyne R P 2003 Plasmon-sampled surface-enhanced Raman excitation spectroscopy *J. Phys. Chem. B* **107** 7426–33
- [5] Dieringer J A, McFarland A D, Shah N C, Stuart D A, Whitney A V, Yonzon C R, Young M A, Zhang X and Van Duyne R P 2006 Surface enhanced Raman spectroscopy: new materials, concepts, characterization tools, and applications *Faraday Discuss.* **132** 9–26
- [6] Metiu H 1984 Surface enhanced spectroscopy *Prog. Surf. Sci.* **17** 153–320
- [7] Le Ru E C and Etchegoin P G 2008 *Principles of Surface-Enhanced Raman Spectroscopy* (Amsterdam: Elsevier)
- [8] Nie S and Emory S R 1997 Probing single molecules and single nanoparticles by surface-enhanced Raman scattering *Science* **275** 1102–6
- [9] Kneipp K, Wang Y, Kneipp H, Perelman L T, Itzkan I, Dasari R R and Feld M S 1997 Single molecule detection using surface-enhanced Raman scattering (SERS) *Phys. Rev. Lett.* **78** 1667–70
- [10] Dieringer J A, Wustholz K L, Masiello D J, Camden J P, Kleinman S L, Schatz G C and Van Duyne R P 2009 Surface-enhanced Raman excitation spectroscopy of a single rhodamine 6G molecule *J. Am. Chem. Soc.* **131** 849–54
- [11] Kleinman S L, Ringe E, Valley N, Wustholz K L, Phillips E, Scheidt K A, Schatz G C and Van Duyne R P 2011 Single-molecule surface-enhanced Raman spectroscopy of crystal violet isotopologues: theory and experiment *J. Am. Chem. Soc.* **133** 4115–22
- [12] Xu H, Bjerneld E J and Börjesson M K L 1999 Spectroscopy of single hemoglobin molecules by surface enhanced Raman scattering *Phys. Rev. Lett.* **83** 4357–60
- [13] Michaels A M, Nirmal M and Brus L E 1999 Surface enhanced Raman spectroscopy of individual rhodamine 6G molecules on large Ag nanocrystals *J. Am. Chem. Soc.* **121** 9932–9
- [14] Xu H, Aizpurua J, Käll M and Apell P 2000 Electromagnetic contributions to single-molecule sensitivity in surface-enhanced Raman scattering *Phys. Rev. E* **62** 4318–24
- [15] Bian R X, Dunn R C and Xie X S 1995 Single molecule emission characteristics in near-field microscopy *Phys. Rev. Lett.* **75** 4772–5
- [16] Camden J P, Dieringer J A, Wang Y, Masiello D J, Marks L D, Schatz G C and Van Duyne R P 2008 Probing the structure of single-molecule surface-enhanced Raman scattering hot spots *J. Am. Chem. Soc.* **130** 12616–7
- [17] Zhang W, Cui X, Yeo Boon-Siang, Schmid T, Hafner C and Zenobi R 2008 Nanoscale roughness on metal surfaces can increase tip-enhanced Raman scattering by an order of magnitude *Nano Lett.* **7** 1401–5
- [18] Becker M, Sivakov V, Andrä G, Geiger R, Schreiber J, Hoffmann S, Michler J, Milenin A P, Werner P and Christiansen S H 2007 The SERS and TERS effects obtained by gold droplets on top of Si nanowires *Nano Lett.* **7** 75–80
- [19] Pettinger B 2006 Tip-enhanced Raman spectroscopy (TERS) *Surface-Enhanced Raman Scattering—Physics and Applications (Topics in Applied Physics vol 103)* ed K Kneipp, M Moskovits and H Kneipp (Berlin: Springer) pp 217–42

- [20] Stöckle R M, Suh Y D, Deckert V and Zenobi R 2000 Nanoscale chemical analysis by tip-enhanced Raman spectroscopy *Chem. Phys. Lett.* **318** 131–6
- [21] Hayazawa N, Tarun A, Inouye Y and Kawata S 2002 Near-field enhanced Raman spectroscopy using side illumination optics *J. Appl. Phys.* **92** 6983–6
- [22] Hartschuh A, Beversluis M R, Bouhelier A and Novotny L 2004 Tip-enhanced optical spectroscopy *Phil. Trans. R. Soc. Lond. A* **362** 807–19
- [23] Bailo E and Deckert V 2008 Tip-enhanced Raman scattering *Chem. Soc. Rev.* **37** 921–30
- [24] Pettinger B, Domke K F, Zhang D, Picardi G and Schuster R 2009 Tip-enhanced Raman scattering: influence of the tip-surface geometry on optical resonance and enhancement *Surf. Sci.* **603** 1335–41
- [25] Tarun A, Hayazawa N and Kawata S 2009 Tip-enhanced Raman spectroscopy for nanoscale strain characterization *Anal. Bioanal. Chem.* **394** 1775–85
- [26] Li J F *et al* 2010 Shell-isolated nanoparticle-enhanced Raman spectroscopy *Nature* **464** 392–5
- [27] Stranik O, Nooney R, McDonagh C and MacCraith B D 2007 Optimization of nanoparticle size for plasmonic enhancement of fluorescence *Plasmonics* **2** 15–22
- [28] Girard C, Martin O J F and Dereux A 1995 Molecular lifetime changes induced by nanometer scale optical fields *Phys. Rev. Lett.* **75** 3098–101
- [29] Chowdhury M H, Ray K, Aslan K, Lakowicz J R and Geddes C D 2007 Metal-enhanced fluorescence of phycobiliproteins from heterogeneous plasmonic nanostructures *J. Phys. Chem. C* **111** 18856–63
- [30] Srituravanich W, Fang N, Sun C, Luo Q and Zhang X 2004 Plasmonic nanolithography *Nano Lett.* **4** 1085–8
- [31] Sundaramurthy A 2006 Toward nanometer-scale optical photolithography: utilizing the near-field of bowtie optical nanoantennas *Nano Lett.* **6** 355–60
- [32] Ozbay E 2006 Plasmonics: merging photonics and electronics at nanoscale dimensions *Science* **311** 189–93
- [33] Atwater H 2007 The promise of plasmonics *Sci. Am.* **296** 56–63
- [34] Frey H G, Witt S, Felderer K and Guckenberger R 2004 High-resolution imaging of single fluorescent molecules with the optical near-field of a metal tip *Phys. Rev. Lett.* **93** 200801
- [35] Novotny L and Stranick S J 2006 Near-field optical microscopy and spectroscopy with pointed probes *Annu. Rev. Phys. Chem.* **57** 303–31
- [36] De Angelis F, Patrini M, Das G, Maksymov I, Galli M, Businaro L, Andreani L C and Di Fabrizio E 2008 A hybrid plasmonic-photonic nanodevice for label-free detection of a few molecules *Nano Lett.* **8** 2321–7
- [37] Anker J N, Paige Hall W, Lyandres O, Shah N C, Zhao J and Van Duyne R P 2008 Biosensing with plasmonic nanosensors *Nature Mater.* **7** 442–53
- [38] Georganopoulou D G, Chang L, Nam J-M, Thaxton C S, Mufson E J, Klein W L and Mirkin C A 2005 Nanoparticle-based detection in cerebral spinal fluid of a soluble pathogenic biomarker for Alzheimer's disease *Proc. Natl Acad. Sci. USA* **107** 2273–6
- [39] Haes A J, Chang L, Klein W L and Van Duyne R P 2005 Detection of a biomarker for Alzheimer's disease from synthetic and clinical samples using a nanoscale optical biosensor *J. Am. Chem. Soc.* **127** 2264–71
- [40] Sherry L J, Jin R, Mirkin C A, Schatz G C and Van Duyne R P 2006 Localized surface plasmon resonance spectroscopy of single silver triangular nanoprisms *Nano Lett.* **6** 2060–5
- [41] Guiton B S, Iberi V, Li S, Leonard D N, Parish C M, Kotula P G, Varela M, Schatz G C, Pennycook S J and Camden J P 2011 Correlated optical measurements and plasmon mapping of silver nanorods *Nano Lett.* **11** 3482–8
- [42] Henry A-I, Bingham Julia M, Ringe E, Marks L D, Schatz G C and Van Duyne Richard P 2011 Correlated structure and optical property studies of plasmonic nanoparticles *J. Phys. Chem. C* **115** 9291–305
- [43] McMahon J M, Gray S K and Schatz G C 2009 Nonlocal optical response of metal nanostructures with arbitrary shape *Phys. Rev. Lett.* **103** 097403
- [44] Coronado E A and Schatz G C 2003 Surface plasmon broadening for arbitrary shape nanoparticles: a geometrical probability approach *J. Chem. Phys.* **119** 3926
- [45] Zuloaga J, Prodan E and Nordlander P 2009 Quantum description of the plasmon resonances of a nanoparticle dimer *Nano Lett.* **9** 887–91
- [46] Zuloaga J, Prodan E and Nordlander P 2010 Quantum plasmonics: optical properties and tunability of metallic nanorods *ACS Nano* **4** 5269–76
- [47] Zhao L, Jensen L and Schatz G C 2006 Pyridine-Ag<sub>20</sub> cluster: a model system for studying surface-enhanced Raman scattering *J. Am. Chem. Soc.* **128** 2911–9
- [48] Jensen L, Zhao L L and Schatz G C 2007 Size-dependence of the enhanced Raman scattering of pyridine adsorbed on Ag<sub>n</sub> ( $n = 2-8, 20$ ) clusters *J. Phys. Chem. C* **111** 4756–64
- [49] Wales D 2003 *Energy Landscapes: Applications to Clusters, Biomolecules and Glasses* (Cambridge: Cambridge University Press)
- [50] Elstner M, Porezag D, Jungnickel G, Elsner J, Haugk M, Frauenheim Th, Suhai S and Seifert G 1998 Self-consistent-charge density-functional tight-binding method for simulations of complex materials properties *Phys. Rev. B* **58** 7260–8
- [51] Aradi B, Hourahine B and Frauenheim Th 2007 DFTB+, a sparse matrix-based implementation of the DFTB method† *J. Phys. Chem. A* **111** 5678–84
- [52] Niehaus T A, Suhai S, Della Sala F, Lugli P, Elstner M, Seifert G and Frauenheim T 2001 Tight-binding approach to time-dependent density-functional response theory *Phys. Rev. B* **63** 085108
- [53] Wang F, Yam C Y, Chen G, Wang X, Fan K, Niehaus T A and Frauenheim Th 2007 Linear scaling time-dependent density-functional tight-binding method for absorption spectra of large systems *Phys. Rev. B* **76** 045114
- [54] Niehaus T A, Heringer D, Torralba B and Frauenheim Th 2005 Importance of electronic self-consistency in the TDDFT based treatment of nonadiabatic molecular dynamics *Eur. Phys. J. D* **35** 467–77
- [55] Krüger Th, Elstner M, Schiffels P and Frauenheim Th 2005 Validation of the DFTB method for the calculation of reaction energies and other data *J. Phys. Chem.* **122**
- [56] Oviedo M B, Negre C F A and Sánchez C G 2010 Dynamical simulation of the optical response of photosynthetic pigments *Phys. Chem. Chem. Phys.* **12** 6706–11
- [57] Oviedo M B and Sánchez C G 2011 Transition dipole moments of the Q<sub>y</sub> band in photosynthetic pigments *J. Phys. Chem. A* **115** 12280–5
- [58] Negre C F A, Fuertes V C, Oviedo M B, Oliva F Y and Sánchez C G 2012 Quantum dynamics of light-induced charge injection in a model dye–nanoparticle complex *J. Phys. Chem. C* **116** 14748–53
- [59] Oviedo M B, Zarate X, Negre C F A, Schott E, Arratia-Pérez R and Sánchez C G 2012 Quantum dynamical simulations as a tool for predicting photoinjection mechanisms in dye-sensitized TiO<sub>2</sub> solar cells *J. Phys. Chem. Lett.* **3** 2548–55

- [60] Niehaus T, Suhai S, Della Sala F, Lugli P, Elstner M, Seifert G and Frauenheim Th 2001 Tight-binding approach to time-dependent density-functional response theory *Phys. Rev. B* **63** 1–9
- [61] Yabana K and Bertsch G F 1996 Time-dependent local-density approximation in real time *Phys. Rev. B* **54** 4484–7
- [62] Runge E and Gross E K U 1984 Density-functional theory for time-dependent systems *Phys. Rev. Lett.* **52** 997
- [63] Schatz G C, Young M A and Van Duyne R P 2006 Electromagnetic mechanism of SERS *Surface-Enhanced Raman Scattering—Physics and Applications (Topics in Applied Physics vol 103)* ed K Kneipp, M Moskovits and H Kneipp (Berlin: Springer) pp 19–46
- [64] Yurkin M A and Hoekstra A G 2007 The discrete dipole approximation: an overview and recent developments *J. Quant. Spectrosc. Radiat. Transfer* **106** 558–89
- [65] Perassi E M, Hernandez-Garrido J C, Sergio Moreno M, Encina E R, Coronado E A and Midgley P A 2010 Using highly accurate 3D nanometrology to model the optical properties of highly irregular nanoparticles: a powerful tool for rational design of plasmonic devices *Nano Lett.* **10** 2097–104
- [66] Perassi E M, Canali L R and Coronado E A 2009 Enhancement and confinement analysis of the electromagnetic fields inside hot spots *J. Phys. Chem. C* **113** 6315–9
- [67] Palik E D 1985 *Handbook of Optical Constant of Solids* (New York: Academic)
- [68] McMahon J M, Wang Y, Sherry L J, Van Duyne R P, Marks L D, Gray S K and Schatz G C 2009 Correlating the structure, optical spectra, and electrodynamics of single silver nanocubes *J. Phys. Chem. C* **113** 2731–5
- [69] Hövel H, Fritz S, Hilger A, Kreibig U and Vollmer M 1993 Width of cluster plasmon resonances: bulk dielectric functions and chemical interface damping *Phys. Rev. B* **48** 18178–88
- [70] Peng S, McMahon J M, Schatz G C, Gray S K and Sun Y 2010 Reversing the size-dependence of surface plasmon resonances *Proc. Natl Acad. Sci.* **107** 14530–4
- [71] Aikens C M, Li S and Schatz G C 2008 From discrete electronic states to plasmons: TDDFT optical absorption properties of  $Ag_n$  ( $n = 10, 20, 35, 56, 84, 120$ ) tetrahedral clusters *J. Phys. Chem. C* **112** 11272–9
- [72] Negre C F A and Sánchez C G 2008 Atomistic structure dependence of the collective excitation in metal nanoparticles *J. Chem. Phys.* **129** 034710
- [73] He Y and Zeng T 2010 First-principles study and model of dielectric functions of silver nanoparticles *J. Phys. Chem. C* **114** 18023–30
- [74] Danckwerts M and Novotny L 2007 Optical frequency mixing at coupled gold nanoparticles *Phys. Rev. Lett.* **98** 026104
- [75] Aeschlimann M, Bauer M, Bayer D, Brixner T, Garcia de Abajo F J, Pfeiffer W, Rohmer M, Spindler C and Steeb F 2007 Adaptive subwavelength control of nano-optical fields *Nature* **446** 301–4
- [76] Huang J S, Voronine D V, Tuchscherer P, Brixner T and Hecht B 2009 Deterministic spatiotemporal control of optical fields in nanoantennas and plasmonic circuits *Phys. Rev. B* **79** 195441